한국동력기계공학회지 제23권 제2호 pp. 66-78 2019년 4월 ISSN 1226-7813(Print) ISSN 2384-1354(Online)
Journal of the Korean Society for Power System Engineering http://dx.doi.org/10.9726/kspse.2019.23.2.066
Vol. 23, No. 2, pp. 66-78, April 2019

Analysis of Nacelle Cover Shape of 250 KW Wind Turbine

Ambarayil Joy Jithin*, Muhammad Sajjad* and Dong-Won Jung**†

(Received 28 January 2019, Revised 18 April 2019, Accepted 22 April 2019)

Abstract: The nacelle is located at the top portion of the wind turbine, and it is the heart part of a wind turbine. Rotors and generators are the major components inside the wind generator which turn the wind energy into rotational power and generate electrical energy. The nacelle cover acts as a protective case and a technical compartment containing these important parts. Nacelle covers that protect these critical parts of wind turbines should be as light as possible, ensuring stability for strength and buckling despite strong winds, and sufficiently supported from wind loads, snow loads and self-weights. Nacelle covers of wind turbines are often used in steel sheets such as galvanized steel sheets to withstand wind and snow loads. The weight is heavy and requires a lot of economic consumption, such as the cost of installation, transportation cost, and increased tower thickness while the steel plate's nacelle cover is stable for the applied load. Recently, many wind turbines have a tendency to use a composite material of a nacelle cover; the composite nacelle cover has a similar strength as steel plate and is lighter than a steel plate, making it economical to consider the production cost of wind turbines. In this paper, we are discussing nacelle cover design process and FEM simulation to determine the shape of a wind turbine under the influence of wind. We are using CFD analysis software 'ANSYS workbench' to determine the shape of the current nacelle cover of the 250 KW wind turbine by changing the shape of the nacelle cover and streamlined shape nacelle cover. This study finds out that there are differences to an influence of wind when wind passes through the nacelle cover because of new shape.

Key Words : Wind Turbine, Nacelle Cover, Snow Load, Finite Element Method(FEM), Computational Fluid Dynamics(CFD)

1. Introduction

Now this time, due to using oil fuel caused environmental pollution. Nuclear energy has good electric power productivity, but nuclear energy has a risk that lect out radioactivity and deals with nuclear waste. According to the United Nations Framework Convention on Climate Change (UNFCCC), countries study how to reduce greenhouse gases.[1] So the world increases interest and study about eco-friendly energy. Wind energy of the eco-friendly energy relatively has good economics.

The wind turbine is a machine for converting the kinetic energy in wind into mechanical energy, then later on this mechanical energy is converted to

**† Dong-Won Jung(ORCID:http://orcid.org/0000-0001-9773-4884): Professor, Department of Mechanical Engineering, Jeju National University.
E-mail : jungdw77@naver.com, Tel ※ 개인정보 표시제한
*Ambarayil Joy Jithin(https://orcid.org/0000-0002-7460-0303) : Graduate studeant, Department of Mechanical Engineering, Jeju National University.
*Muhammad Sajjad)https://orcid.org/0000-0002-4897-079X): Graduate studeant, Department of Mechanical Engineering, Jeju National University.

electricity. Wind turbines are mounted on the top of the tower to capture most of the wind energy. The working of the wind turbine, blades of the turbine act like wings of an airplane capturing the energy in the wind. The blades cut through the air with an angle of attack to the wind causing a pressure differential.[2–3] The resulting pressure differentials cause a force called lift which propels the blade forward. This lift is created because of the airfoil shape of the turbine's blades. In order to propel the turbine, the net torque caused by lift forces must be greater than the net torque caused by drag forces.[4] The blades turn a generator that converts blade rotation into electricity the tail help keeps the blades facing the wind. The schematics of a wind turbine and there working are shown in Fig.1. In the chemical process industry, efficient gas-liquid contacting is essential in processes such as hydrogenation, chlorination, etc. Gas-liquid interfacial mass transfer often controls the overall production rate of the gas-liquid reactors. High-intensity gas-liquid mixers, like static mixers, rotor-stator and ejector are increasingly used as a primary gas dispersion device in a gas-liquid reactor. These high intensity mixers can improve the mass transfer rates by generating small bubbles, which are then injected into a reaction vessel, thereby improving the mass transfer characteristics of the entire system.

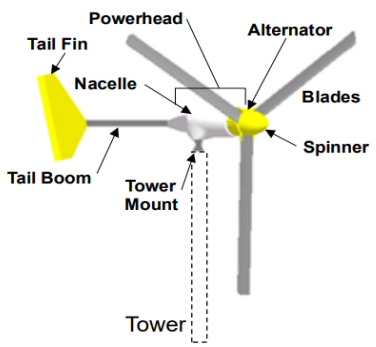

Fig. 1 Schematic diagram of Wind Turbine

A wind turbine is composed of a rotor, nacelle, and tower. Nacelle is an important part of wind turbine that produces electric power, so nacelle must be kept in safe from bad weather conditions.

For this reason, in order to design the shape of nacelle cover which is less influenced by wind, we are using CFD analysis for the designing and simulation of nacelle cover. The modification consists of changing the external shape of nacelle cover and the streamlined shape of nacelle cover.[5-7]

Previously many researcher work on flow field characteristics of wind tunnel, Jang Kweon Kim studied about the numerical analysis of internal flow field characteristic of wind tunnel using Morel's curve equation.[8] Later in next year they extended there study and investigate the flow field characteristics of these tunnel according to the change of contract length.[9] But these cover are rectangular in shape and are made of galvanized steel plates. The weight of wind generator components is classified as heavy, which leaves room for improvement in lightness. The material considered to be replaced as composite materials, which can be used to reduce the costs by replacing with a relatively cheaper composite material than the traditional galvanized steel plate.[10] And using composite materials to lighten the weight, reducing shipping and installation costs to the installation site of wind turbines after production. In addition to the, additional effects of lightning may be possible to change the structure and material of the tower, which may expected to lead the additional cost savings.

2. 3D Modeling of Existing Nacelle Covers

For the analysis of nacelle covers, 3D modeling was first performed and the design was reverse-engineered to produce 2D drawings. In order

to compare the results derived from the simulation analysis of the existing and newly developed nacelle covers in the simulation analysis, 3D modeling was performed for the existing nacelle covers and the two anticipated nacelle covers.

When a nacelle cover, no bolts and hinges connecting the nacelle cover to the upper cover expected to directly affect the interpretation.

Existing 3D modeling of nacelle covers used in 250 kW wind farms owned by participating companies was modelling. Shell modeling was performed using the surface function of the structured program to measure each part, and 3D modeling was performed for each of the five parts as appeared in Figure 2.

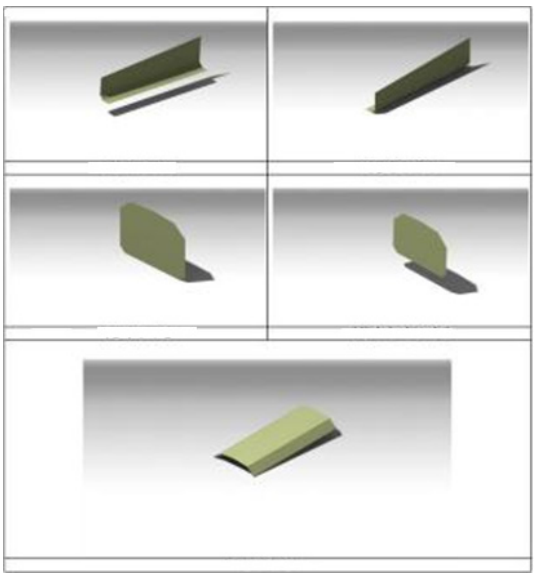

Fig. 2 Existing nacelle cover 3D modeling

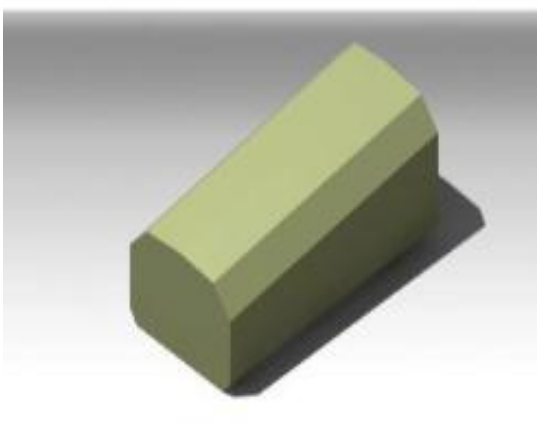

Fig. 3 Assembly of the nacelle covers existing

Figure 3 demonstrates an assembly of each of the six 3D modelled parts, referring to the measured dimensions. Although the bolts are actually assembled for fixing each part, the bolts are omitted in the simulation analysis so that a quick and accurate interpretation can be made through a simplified analytical model.

As the Nacelle cover of a 250 kW class wind generator have some limitations on changing the shape, it will be made to existing model accordingly. As the material is changed from galvanized steel plates to composite materials, a new shape will be enforced with emphasis on material stiffness issues. One of the ways to increase rigidity in reality without increasing thickness of current nacelle covers is to formulate aboard. For example, features such as corrugated or slate roofs were considered to be more resistant to external forces. The analysis program was used to determine the number of beads on the upper and lower sides, by providing curved folds and smooth fillets on each part, such as side and upper covers, to reduce the impact of wind flow.

Table 1 Number of nodes and elements depending on the number of beads

Number of beads	Node	Element
0	8,726	8,529
1	14,525	14,329
3	22,288	21,985
5	29,486	29,167
7	35,598	35,265

3. Experimental results and discussion

3.1 Establishing and interpreting conditions for determining lateral geometry

New model consists of 4,000mm wide, 1,900mm long, and 3t thick models were modeled using analytical software. As shown in Table 1. the number of beads has been given 0, 1, 3, 5, and 7, and the number of points and elements according to the number of beads. The number of beads was determined to be dependent on the area of the side cover, and a maximum of seven beads could be given.

For the above analysis FRP material properties, which is commonly used in composite materials and the physical properties have appeared in Table 2. The thickness of each plates are 3 mm and a load of 2,000 N corresponding to the wind speed of 25m/s. The results are derived from the above conditions, and the simulation results are derived from stress, deformation, and strain.

The numerical analysis directed towards modelling the same ejector geometry used in experiments in order to compare results. Figure 4 shows that, when the number of beads is zero, the stress is concentrated at the edge of area fixed for analysis, so the stress is concentrated at the center point and gradually dispersed from both edges. As the number of beads increases, the distribution of stress is shown as a circular shape. As shown in Fig. 5, the stress decreases due to the increase of beads.

Strain is derived as a result similar to stress.

Table 2 Properties of FRP

Density	Poisson's ratio	Modulus of elasticity	Tensile strength
1.5g/cm^3	0.38	165 GPa	705 MPa

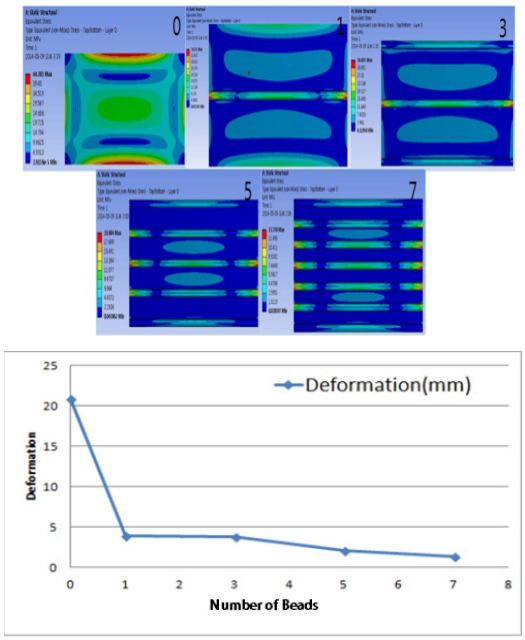

Fig. 4 Stress values and graph according to number of beads

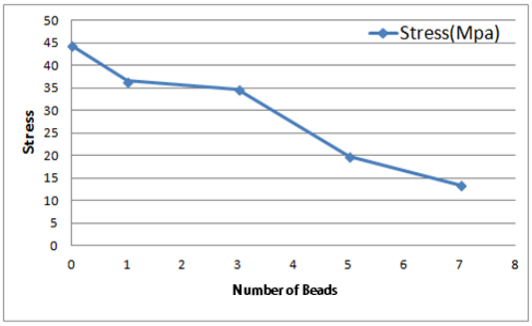

Fig. 5 Strain graph by number of beads

Table 3 Result values of stress, strain, and strain based on the number of beads

	0	1	3	5	7
Stress (MPa)	44.381	36.551	34.693	19.904	13.378
Defor-mation (mm)	20.837	3.9162	3.8466	2.0502	1.3646
Strain	0.0002 6898	0.0002 243	0.000 213	0.0001 2252	0.0000 82412

The strain is concentrated at the edge for interpretation when there is no bead, but the elongation of the bead results in a distribution of the concentrated strain at the edge of the bead, resulting in a reduction in strain.

The results values for stress and strain shows that the number of beads increases, each result value are decrease, and the correct value for each analysis result is shown in Table 3. The number of beads on the side cover of the nacelle is determined based on the above simulation analysis values.

3.2 Condition and analysis for top geometry determination

The material properties of the sides and the plates, the thickness and size, the boundary conditions, and the applied load are the same as the determination of the existing side shape, and the number of blocks and elements is shown in Table 4.

The side and upper face analysis results tend to be similar. As Figure 6 shows the stress is concentrated at the fixed upper and lower edges, and can see that the more bead, the more distributed it is. When there are 16 beads, it is possible to see that the stress distributed across both edges of the bead is concentrated. Referring to Figure 7, the number of beads has decreased from 8 to a lower slope for stress reduction, and there has been no significant stress reduction between 12 and 16.

Table 4 Number of nodes and elements depending on the number of upper beads

Number of beads	Node	Element
0	8,726	8,529
4	14,525	14,329
8	22,288	21,985
12	29,486	29,167
16	35,598	35,265

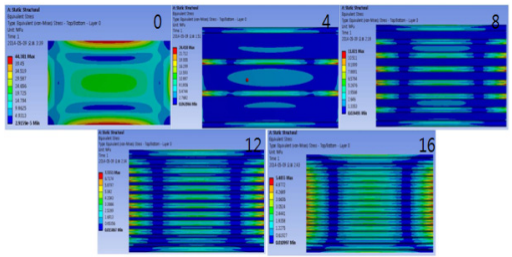

Fig. 6 Stress values according to the number of beads

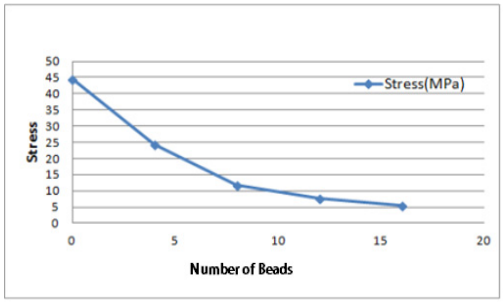

Fig. 7 Stress graph with number of beads

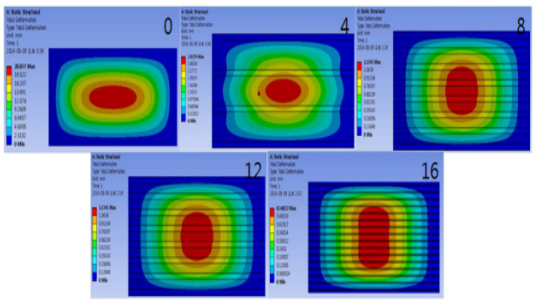

Fig. 8 Strain values according to thenumber of beads

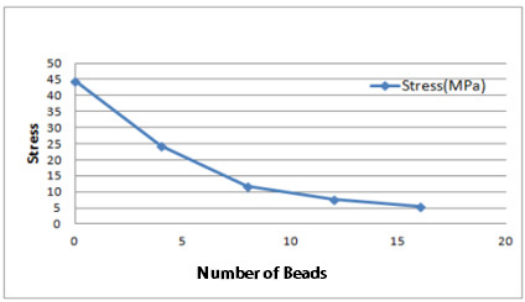

Fig. 9 Strain graph by number of beads

Table 5 Stress, strain and strain result values according to the number of upper beads

	0	4	8	12	16
Stress (MPa)	44.381	24.418	11.821	7.5551	5.4855
Deform-ation (mm)	20.837	2.9279	1.1743	0.73576	0.54022
Strain	0.0002 6898	0.000 15021	0.0000 71851	0.0000 45955	0.0000 33345

Each resulting value confirmed that the stress values decreased as the number of beads increased, and the resulting values did not differ significantly between 12 and 16. The shape of the new nacelle cover was determined by considering he area above the nacelle.

4. Determining the New Geometry of the Nacelle Covers

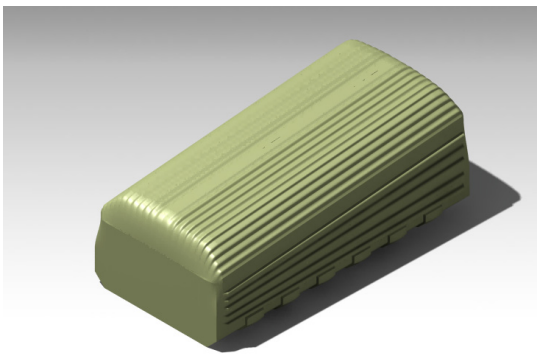

Fig. 10 Prefabricated nacelle cover

4.1 3D design of nacelle Covers with hardwired geometry

The beaded nacelle cover will be used on a 250 kW wind generator, so the overall dimensions will not vary much. 3D modeling of the bead-shaped nacelle cover was performed with reference to the existing 2D drawing and 3D modeling of the nacelle cover.

The shell was modeled to speed up the analysis of the nacelle cover, and the assembly of each part was assembled after matching each part with the edges. The front or back of the nacelle cover is covered by a hub, and the front and back sides are less areas than the left and right sides, so the bead was not added.

5. Structural Analysis of Existing Nacelle Cover

Analysis of Nacelle Cover was carried out by analyzing current Nacelle Cover and wired Nacelle Cover. The loads were then analyzed using two types of loads, one is wind and the other one is snow load, referring to the G.L Guide. The material properties were galvanized steel plates and FRP materials, and composite specimens were manufactured directly and analyzed using the results of tensile testing. Existing nacelle cover structural analysis was performed using galvanized steel plates and FRP material properties. By using this analysis, the resultant weight of the existing nacelle cover was compared.

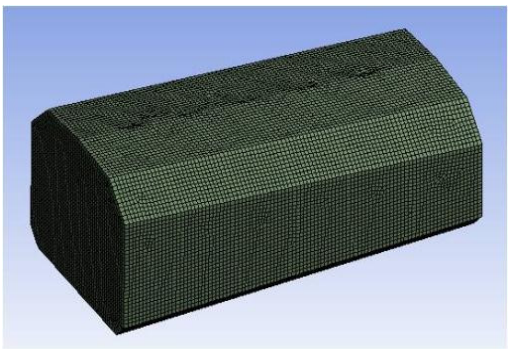

Fig. 11 Splitting the mesh

5.1 Finite modeling of existing nacelle cover

For this structural analysis, the existing 3D modeling of the nacelle cover was modified. Using the design program, the connections between the

nacelle and the nacelle face entering the interior of the nacelle cover are modelled as shown in Figure 11. It shows that, the constraints for the simulation analysis and it was judged that the load would actually be tightened and supported in the same place as the brackets on the internal skeleton, thus applying these boundary conditions. It is assumed that there is a virtual holding bar in the area where the boundary condition is imposed.

Existing nacelle covers are not complex and have Hexa Mesh applied for fast Mesh setting. The number of split points and elements is 21,823 and 22,604, respectively.

5.2 Analysis of existing nacelle cover with zinc plated steel plates

The applied load on the nacelle cover are shown in Equation (1) using the wind load equation shown in the G.L Guide, and the area and wind velocity of each side of the existing nacelle cover. The same force is applied to an analysis using FR physical properties.

Simulation analysis were performed under the above wind load conditions, and the corresponding stress, strain values and strain rates are shown in Table 7, with the distribution according to the resulting values shown in Figures 12 and 13.

When analysed using the galvanized steel plate material properties, each resulting value was seen to increase with increasing wind velocity, and the maximum value of each result was seen to act on the right-hand front.

Table 6 Wind load on existing nacelle covers

	5	10	15	20	25
Front	31.3	125	281.3	500.1	781.4
Back	31.3	125	281.3	500.1	781.4
Top and bottom	80.2	320.9	722.1	1283.8	2005.9
Side	51.6	247.9	464.8	826.4	1291.2
Side (wind)	82.6	330.6	743.7	1322.2	2066

Table 7 Analysis results of nacelle covers using galvanized steel sheets

	5	10	15	20	25
Stress (MPa)	3.2579	3.2207	4.9915	7.4872	10.696
Deformation (mm)	0.19499	0.22861	0.35549	0.53324	0.76176
Elastic strain	$1.55E^{-5}$	$1.57E^{-5}$	$2.43E^{-5}$	$3.65E^{-5}$	$5.21E^{-5}$

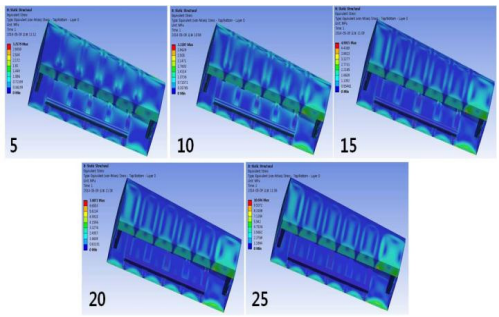

Fig. 12 Stress results from galvanized steel plate

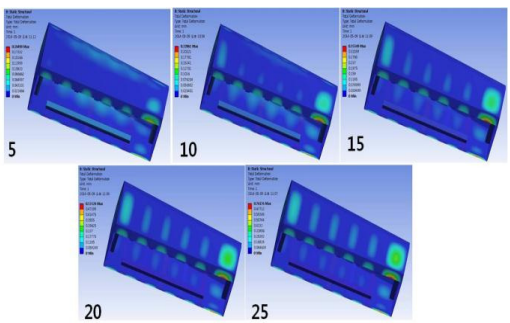

Fig. 13 Strain results from galvanized steel plates

5.3 Analysis of FRP physical properties and snow removal under existing nacelle cover

Unlike the wind load, structural analysis applied with snow cover applied load only to the upper cover of the existing nacelle cover. This snow load was applied in the G.L Guide by using Equation (2) for Snow Removal and the upper projection area of the existing nacelle cover.

$$P_{sk} = 3.0 \cdot \mathrm{kN/m^2}$$

The existing Nacelle cover is 2.05 m long and 4.26 m long, the area is 8.733m2 and the snow load is 26.2 kN, when the area is divided by 3.0 kN. The structural analysis applied with this snow load is the same as the structural analysis performed previously except for the load.

The results of the structural analysis applied with snow load are shown in Table 8, and the distribution of the results is shown in Figures 14.

Table 8 Results of structural analysis of existing nacelle covers with FRP material properties and snow load

	STRESS (MPa)	STRAIN	DEFORMATION (mm)
Result Value	126.2	0.00076618	1.1091

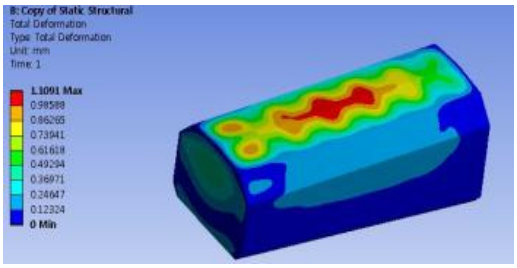

Fig. 14 Strain value of structural analysis applied with snow load

In the structural analysis applied with snow cover, the strain value is concentrated at the center of the upper cover of the nacelle and is shown up to 1.1091mm. The remaining stress and strain values are shown in the upper cover of the nacelle.

6. Structural Analysis of Wired Nacelle Cover

6.1 Finite element modeling of linear nacelle cover

No additional 3D modeling was performed in the structural analysis of the wired nacelle cover. The bottom edge of the wired nacelle cover was fixed. As shown in Figure 15, a wired nacelle cover is fitted with a bead on the wire type and the nacelle cover plate. Mesh has 203,858 and 406,056.

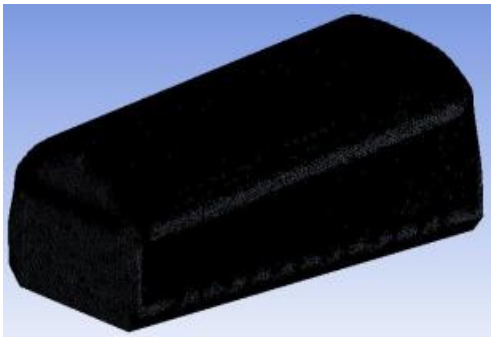

Fig. 15 Mesh in a wired nacelle cover

6.2 Load and physical properties for structural analysis if wired nacelle cover

Wind load and magnification, such as the existing nacelle cover, are applied to the wired nacelle cover. Wind load depends on the projection area and the constant Cw along the direction of the wind and the speed of the wind on the nacelle cover. The value for Cw is the constant value due to the wind blowing in the direction of the wind, in the front or in the side.

The material properties to be used for wire-type nacelle covers are the same as the FRP property properties used for structural analysis.

6.3 Simulation of wired nacelle cover

The conditions used in existing nacelle covers have been simulated and the corresponding stresses strains are shown in Table 10. The result values show that, each result value decreases as it moves over to 5 to 10 m/s. Stress and strain values are shown to be concentrated in the lower part of the side.

Table 9 Physical properties to be used for wired nacelle covers

	Density (g/cm^3)	Poisson's Ratio	Elasticity factor (GPa)	Tensile strength (MPa)
FRP	1.5	0.38	165	705

Table 10 Wired nacelle cover analysis results

	5	10	15	20	25
Stress (MPa)	8.5793	3.3113	7.7759	13.471	20.792
Defor-mation (mm)	1.6193	0.68321	1.2852	2.1724	4.4183
Elastic strain	$5.71E^{-5}$	$2.20E^{-5}$	$5.14E^{-5}$	$8.74E^{-5}$	$1.43E^{-4}$

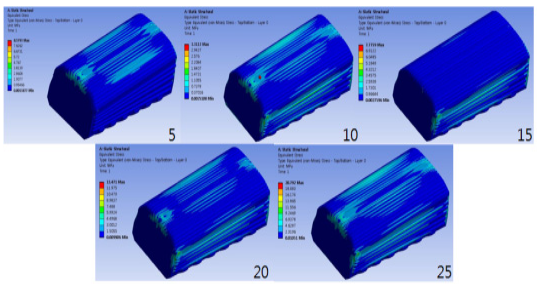

Fig. 16 Stress according to wind speed

Based on the result deformation, the reason why the maximum value is higher than the side is because the upper part receives more magnetic force than the wind load.

6.4 Structural analysis using snowfall load of wired nacelle cover

Wired nacelle covers are expected to take a long time because they have additional wired and bead, and the snow load only applies to the upper cover of the nacelle cover, excluding the upper part of the nacelle cover.

The Tetra mesh used which has 18,224 points and 35,948. The mesh can be seen around the upper bead.

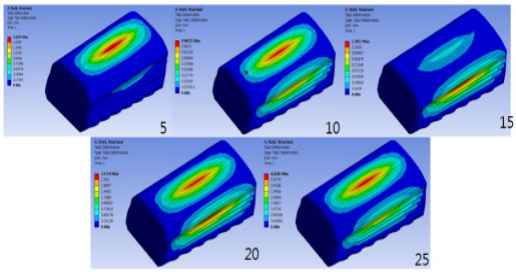

Fig. 17 Transformation according to wind speed

Table 11 FRP Physical Properties

	Density (g/cm^3)	Poisson's Ratio	Elasticity factor (GPa)	Tensile strength (MPa)
FRP	1.5	0.38	165	705

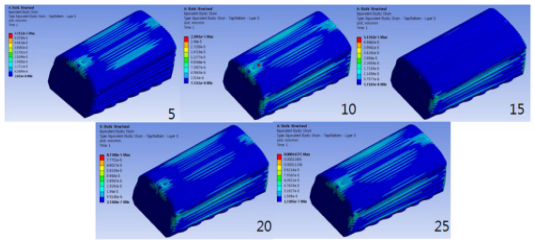

Fig. 18 STRAIN according to wind speed

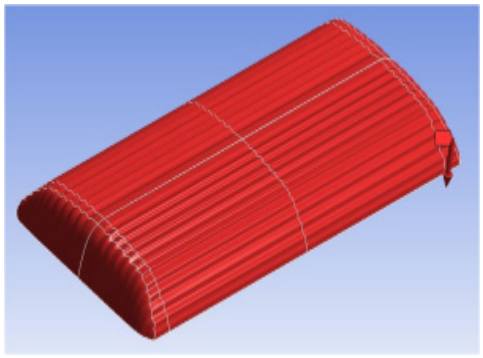

Fig. 19 Illustration of snow load application

Table 12 Analysis result of wired nacelle cover snow load

	Stress	Strain	Deformation
Result Value	230.26	0.00169	75.9

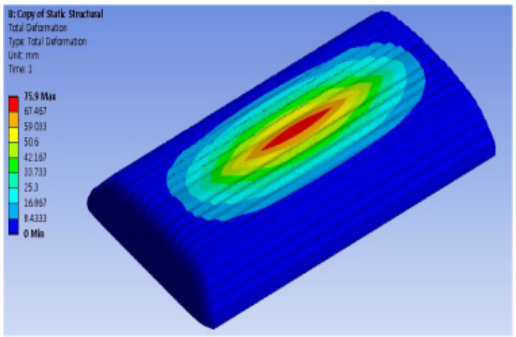

Fig. 20 Deformation

The material properties of the wired nacelle cover are identical to those of the FRP of the existing nacelle cover, and the snow load are same as those of the G.L. Guide. The upper projection area of the wired nacelle cover is 2.05 m wide and 4.27 m long, and the snow load is 26.28 kN.

The resulting values for a hardwired nacelle cover with snow load are shown in Table 11. and the distribution according to the resulting values is shown in Figures 20.

Each result value shows that the strain is concentrated in the center of the cover and that the stress and strain are spread widely at the top edge.

7. Wired Nacelle Cover Wind Load Simulation

As a result of the tensile test, a wired nacelle cover analysis with bead shapes was conducted. The physical properties are the same as in the 3rd simulation analysis, and the load was calculated 5 m/s from 5 m to 25 m/s using the wind load expression in the G.L Guide, and the wind load is shown in Table 6. We added weights like wind loads. The magnification used the Standard Earth Gravity function of the analysis program.

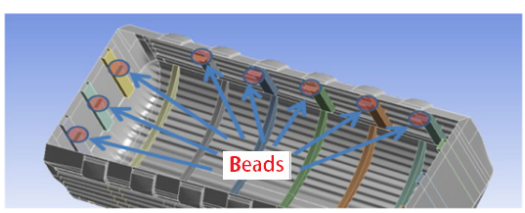

Fig. 21 Nacelle Cover Fasteners-2

Inside the nacelle cover, parts that are connected to the nacelle on both sides and front and rear are added as shell modeling, which is secured using the Fixed function. The bead-shaped, wired nacelle cover provides a tetra mesh, and the Auto mesh results in an error between the nacelle cover and the inner support. Using the contact function between the nacelle cover and the inner support, Mesh is connected. Mesh has 234,682 points and 446,022 elements.

The simulation analysis results show that the strain, 10 m/s, and the stress and strain are reduced to 15 m/s, depending on where the maximum value of each result appears. Figures 56 through 58 show a decrease in the presence of maximum values in the front or back.

8. 3D Printing Models

Table 13 Analysis results by wind load

Wind (m/s)	5	10	15	20	25
Deformation (mm)	0.54774	0.51761	0.84395	1.4716	2.2786
Strain	0.00035015	0.00032356	0.00026993	0.00040754	0.00061951
Stress (MPa)	4.7294	4.3716	3.8717	4.9567	7.5853

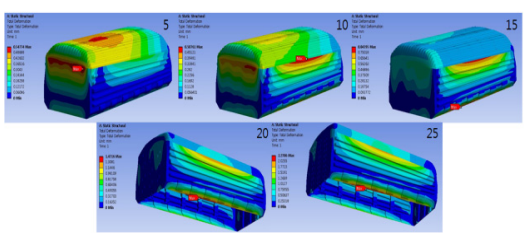

Fig. 22 Strain - Maximum location according to wind amount

To observe the overall shape of the product, a 3D printer was used to create a prototype type. 3D printing technology now has many advantages, including the ability to identify problems with real-life products by producing identical prototypes with cheap, easy-to-mold materials.

In this research, the above technology was introduced and applied to detect possible problems such as assembly by printing out the entire shape prior prototype production. Existing 3D modeling files were converted to STL-files and applied to 3D printer-specific software. Within the software, only nacelle shapes developed after geometry review were printed.

The 3D printers used are shown in Figure 24 from 3D SYSTEM. When printing the nacelle cand are output using CUBEX TRIO X modelsover, it is output by a plastic jet printing method, which is one of the rapid prototyping methods, and is manufactured using two materials: ABS and PLA plastic.

Figure 25 below shows the nacelle features printed using the above 3D printer. Due to limitations of the 3D printer function, it was not possible to separate and assemble the parts of the nacelle cover divided into 6 parts (or pieces) and manufactured them entirely with one part, nacelle cover. By printing the nacelle printed features, we were able to increase our understanding of the overall contours and features, and we were able to confirm that the 3D-modeled CAD files based on the nacelle 2D drawings were also correctly designed.

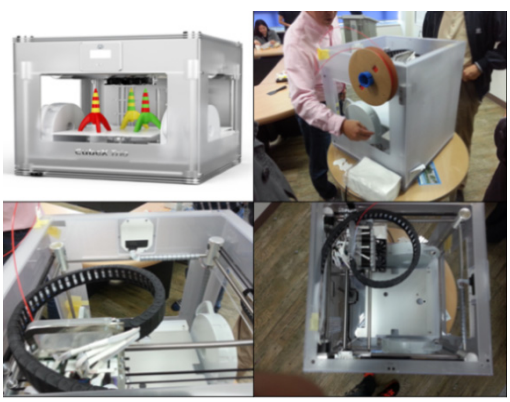

Fig. 24 3D printer devices used in nacelle shape

Prior to production of Nacelle Covers, the dimensions of the nacelle cover were reviewed by using a 3D printer, and if the prototype is manufactured considering tolerances from the components of the connection such as hinges, it is deemed possible to produce a nacelle cover with accurate dimensional accuracy.

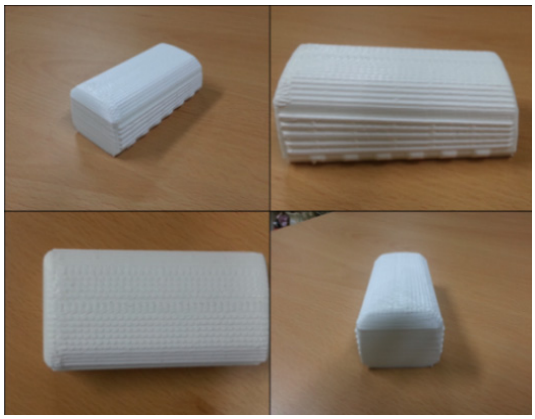

Fig. 25 3D printer nacelle shape

9. Conclusion

The objectives of this project are to develop a nacelle cover for wired composite materials, FEM simulation analysis, composite nacelle production, and product evaluation. The FEM simulation includes the design and modeling process, and 2D drawings and 3D modeling were derived through the paradox of the wired nacelle cover with reference to the existing nacelle geometry. Wired nacelle covers have the addition of wrinkled beads to enhance the stiffness of the nacelle cover, and a structural analysis according to the number of folds was performed to determine the appropriate shape and

number of wrinkles. The final form of the wired nacelle cover was derived through the above structural analysis, wind load analysis, and snow load analysis was performed to compare the performance of the nacelle cover developed with the existing nacelle. In the manufacture of composite nacelle cover, the validity of the composite material's process was reviewed through specimen manufacture, and the tensile strength and surface illumination values of the composite material were checked through the certification test institution after specimen. The manufacture of a composite nacelle cover was performed after confirming that the tensile strength and surface illumination of the composite material was achieved through a specimen test.

The nacelle cover features used dimensions of features considered to be valid during the design and modeling process and simulation process, and the fabrication process produced a wired composite nacelle referring to the production process of composite materials validated through specimen testing. The developed nacelle cover consists of six parts, not a single unit, and the dimensional accuracy of each part is required to be checked during the assembly process. It was installed directly on the 250 kw wind generator Nacelle to be installed. In the product evaluation process, the measurement of three items, including lightning, surface illumination, and tensile strength, was reviewed and the product target value was met. The above process was used to manufacture nacelle covers for wired composite materials. Based on this development technology, it is deemed that it is applicable to new nacelle cover features and other fields, and by conducting additional research on composite materials manufacturing technology, it is possible to develop high-quality composite materials suitable for use.

Author contributions

D. W. Jung; Writing-original draft. A. J. Jithin; Investigation. M. Sajjad; Formal analysis.

References

1. J. Y. Lee, N. J. Choi, H. Y. Yoon, I. S, Kim and Y. D. Choi, 2010, "Design and Flow Analysis on the 1 kw-Class Horizontal Axis Wind Turbine Suitable for Islands Region", Korean Society for Fluid Machinery, Vol. 15, pp. 472-473. (DOI:10.5293/kfma.2012.15.3.005)
2. A. Goto, 1992, "Study of internal flows in a mixed-flow pump impeller at various tip clearances using three-dimensional viscous flow computations", ASME Journal of Turbo-machinery, Vol. 114, pp. 378-382. (DOI:10.1115/1.2929154)
3. W. N. Dawes,, 1986, "A numerical method for the analysis of three dimensional viscous compressible flow in a turbine cascade: Application to secondary flow development in a cascade with and without dihedral", ASME Paper 86-GT-145. New York: American Society of Mechanical Engineers, Vol. 1, pp. 59-66. (DOI:10.1115/86-GT-145)
4. J. H. Kim, B. S. Kim, C. D. Nam and Y. H. Lee, Y. H., 2003, "A Study on Flow Analysis and an Estimate of Performance for HAWT by CFD", Journal of the Korean Society of Marine Engineers, Vol. 27, pp. 906-913.
5. B. P. M. van Esch, N. P. Kruyt and J. B. Jonker, 1997, "An inviscid-viscous coupling method for computing unsteady flows in entire pump configurations", The ASME Fluids Engineering Division Summer Meeting, FEDSM'97, June 22-26, pp. 1-8.
6. B. S. Lee and Y. H. Kim, 2006, "A Study on

the Flow and the Aerodynamic Performance Analysis on the 20kW HAWT by CFD", Proceedings of The Fourth National Congress on Fluids Engineering, pp. 1243-1246.

7. Y. T. Nam, B. S. Kim, J. H. Kim, C. D. Kim and Y. H. Lee, 2003, "A Study on Evaluation fo the Application of a CFD Code to Flow Analysis and an Estimate of Performance for HAWT", The Korean Society of Mechanical Engineers Spring Conference, pp. 2192-2197.
8. J. K. Kim and S. H. Oh, 2018, "Numerical Analysis on the Internal Flow Field Characteristics of Wind Tunnel Contractions with Morel's Equation", The Korean Society for Power System Engineering, Vol. 22, pp. 11-17. (DOI:10.9726/kspse.2018.22.1.011)
9. S. H. Oh and J. K. Kim, 2018, "Numerical Analysis on the Internal Flow Field Characteristics of Wind Tunnel According to the Change of Contraction Length", Journal of the Korean Society for Power System Engineering, Vol. 22, pp. 81-88,
10. B. Thwaites, 1948, "Approximate calculation of the laminar boundary layer", The Aeronautical Quarterly, Vol. 1, pp. 245-280. (DOI:10.1017/S0001925900000184)